Band gaps, effective masses and refractive indices of PbSrSe thin films: Key properties for mid-infrared optoelectronic device applications

W. Z. Shen,[a] H. F. Yang, L. F. Jiang, K. Wang, and G. Yu
Department of Physics, Laboratory of Condensed Matter Spectroscopy and Opto-Electronic Physics, Shanghai Jiao Tong University, 1954 Hua Shan Road, Shanghai 200030, People's Republic of China

H. Z. Wu and P. J. McCann
School of Electrical and Computer Engineering, and Laboratory for Electronic Properties of Materials, University of Oklahoma, Norman, Oklahoma 73019-1023

(Received 13 June 2001; accepted for publication 3 October 2001)

Key properties of PbSrSe thin films grown by molecular beam epitaxy have been studied for mid-infrared optoelectronic device applications. Detailed knowledge of the material parameters for the device design is required. The material parameters considered are: temperature-dependent band gaps, composition (or band gap)-dependent effective masses, and energy-dependent refractive indices. The study has been carried out by a combination of temperature-dependent photoluminescence and absorption measurements with the theoretical models on PbSrSe thin films of Sr compositions of as high as 0.276. The derived empirical equations for band gaps, effective masses, and refractive indices have been employed successfully in PbSe/$Pb_{0.934}Sr_{0.066}Se$ multiple quantum well mid-infrared laser systems, for studying the band offsets and subband behavior. We have shown that the derived material parameters clearly promise of being applied to other PbSrSe thin films and PbSe/PbSrSe heterostructure systems for their optoelectronic applications. © *2002 American Institute of Physics.* [DOI: 10.1063/1.1421634]

I. INTRODUCTION

Recently, considerable interest has been devoted to the lead salt IV–VI PbSe-based materials because of their potential optoelectronic applications. Alloying Sr into PbSe can significantly increase the band gap energy of $Pb_{1-x}Sr_xSe$.[1,2] The wide tuning range of the energy bands within the ternary system,[1,2] together with the ease in producing good quality material with excellent homogeneity and small lattice mismatch on BaF_2 substrates,[1] and the possibility of epitaxial growth on Si substrates,[3] has provided PbSrSe the basis for devices operating over the wide mid-infrared wavelength range, particularly useful for mid-infrared intrinsic detectors and lasers. The material has a multi-valley band structure with band extrema at the *L*-point of the Brillouin zone. The absence of a heavy-hole band reduces the nonradiative Auger recombination rate, one or two orders of magnitude below that of narrow gap III–V and II–VI materials,[4,5] which is favorable for the reduction of the high temperature threshold current. Lower density of states and stronger interband matrix elements allow the appearance of stimulated emission at relatively low generation rates. Strong continuous-wave room temperature stimulated emission luminescence has been observed[4,5] between 3.0 and 4.0 μm from PbSe/PbSrSe multiple quantum well (MQW) structures, well above the limit of 2.3 μm in type II quantum cascade laser structures using narrow gap III–V antimonide semiconductor materials. However, design of optoelectronic devices in such PbSrSe systems has been hampered by a lack of definite knowledge of many material parameters.

The motivation of the present study for PbSrSe and their microstructures has been provided by the fact that the fundamental properties, including some important parameters, have not been fully investigated. Lambrecht *et al.*[1] presented a number of important material parameters for PbSrSe, e.g., the room temperature band gaps, lattice constants, mobilities, and carrier concentrations. The parameters to be presented here are: temperature-dependent band gaps, composition (or band gap)-dependent effective masses, and energy-dependent refractive indices. The measurements employed have been temperature-dependent photoluminescence (PL) and absorption measurements for PbSrSe thin films grown by molecular beam epitaxy (MBE). The band gap energy, especially its temperature dependence, is known to be one of the most important device parameters because it is strongly connected with the operating wavelength of optoelectronic devices. Determining the effective mass and the band offset and knowing the subband characteristics are central for the study of semiconductor heterostructures and superlattices as well as their optoelectronic applications. Knowledge of the refractive index also forms an important part in the design of heterostructure lasers, as well as other waveguiding devices.[6]

On the other hand, until now, the optical investigation in the literature has been limited to the narrow band $Pb_{1-x}Sr_xSe$ materials with the largest Sr composition of $x \leqslant 0.2$.[1,2,7] This article will present experimental results of PbSrSe thin films with Sr compositions of as high as 0.276. This enables us to obtain information on the optical constants over much wide spectral range, since the energy gap increases rapidly with the Sr composition. The resultant analytical expressions for temperature-dependent band gaps, composition (or band gap)-dependent effective masses, and

[a]Electronic mail: wenzshen@sina.com

energy-dependent refractive indices are used for comparison with the reported results in the literature, and to study the band offsets and the subband behavior in PbSe/PbSrSe MQW mid-infrared laser systems with Sr composition of 0.066, by taking into account the strain, carrier confinements and the multi-valley band structure. A good agreement with the reported experimental results in the literature has been found, which clearly promises that the results obtained here are applicable to other PbSrSe thin films and PbSe/PbSrSe heterostructure systems for their optoelectronic applications.

II. EXPERIMENTS

Three PbSrSe thin films were grown on freshly cleaved BaF_2 (111) substrates by MBE techniques in an Intevac GEN II Modular system. PbSe, Se and Sr were used as source materials, and the Sr concentration in PbSrSe films was determined from the beam equivalent pressure (BEP) ratios of the Sr and PbSe fluxes during MBE growth. Sr–to–PbSe flux ratios of 2.9%, 7.4% and 12.0% were employed to grow the three PbSrSe thin films, which resulted in Sr compositions of 0.066, 0.171, 0.276, respectively.[5,8] There is about −12% BEP calibration error (within the uncertainty of the calibration[1]) in our MBE system due to the different concentration gradients across the sample holder in different MBE facilities, based on the calibration of Lambrecht *et al.*[1] The thin films had layer thickness of around 1μm. The 40 periods PbSe/PbSrSe MQW mid-infrared laser systems employed to validate our results were also grown by the same MBE facility on the same BaF_2 (111) substrates. The MQW had the well layer thickness of 40–200 Å and barrier layer thickness of 400–500 Å with the Sr composition of 0.066 in the barriers. Details of the growth techniques and photoluminescence (PL) measurements for PbSe/PbSrSe MQW structures were published elsewhere.[4,5] The temperature-dependent PL and absorption measurements for the PbSrSe thin films were performed on a Nicolet Nexus 870 Fourier transform infrared (FTIR) spectrometer, with liquid nitrogen cooled InSb detector, and a 532 nm laser as the excitation source for PL and a globar infrared source for absorption. The optical measurements were made at the resolution of 4 cm^{-1}.

III. TEMPERATURE-DEPENDENT BAND GAPS

Figure 1 shows the PL and absorption spectra at 10 K for the $Pb_{0.934}Sr_{0.066}Se$ thin film. In the PL spectrum, a single PL peak is observed throughout the temperature range of the measurements (10–300 K). The strong room temperature luminescence observed demonstrates the good quality of the sample. A systematic study[8] of the dependence of the luminescence spectra on the excitation intensity and temperature reveals four distinct features. At low temperature, the spectra (1) get narrower, (2) shift the peak to low energy, (3) get increasingly asymmetric with the decrease of excitation intensity, and (4) the luminescence intensity increases (unusually) up to the temperature of 100 K and then decreases (as normally expected) with the increasing temperature. Based on these, the single luminescence structure has been attributed to localized excitonic line due to the alloy disorder at low temperature, and is gradually delocalized as band-to-band transitions at high temperature.[8,9] The full width at half maximum (FWHM) is 12.1 meV at 10 K and 67.4 meV at 300 K. In the absorption spectrum, a clear absorption edge is observed followed by below band gap Fabry-Pérot interference fringes. The absorption edge increases with the temperature, as expected, in the whole measured range. The atmospheric CO_2 absorption structures are also displayed in the absorption spectrum. The absorption edge energies can be obtained, as widely employed in the literature,[10,11] from the intersection of the square of the absorption slope with the lowest measured absorption between the interface fringes. Shown in the inset of Fig. 1 is the band gap energies (E_g) of the PbSrSe thin film, as derived from both absorption and PL measurements (via correction due to the band-to-band PL transition above 100 K). It is found that little Burstein–Moss effect is observed in the undoped PbSrSe thin film grown by MBE due to low carrier concentration, in contrast to the case for lead salts grown by other methods, such as liquid phase epitaxy.[10] The best fit of the experimental results for the $Pb_{0.934}Sr_{0.066}Se$ thin film gives $E_g = 382.4 + 0.2542\,T$ (meV). The obtained E_g expression for room temperature agrees well with reported values.[1,5] The band gaps are found to be linear with the temperature in all three thin films, the same as in the ternary system of HgCdTe.[12] The temperature coefficient dE_g/dT decreases with the increase of Sr content (0.2542, 0.0902, and 0.0712 meV/K for the Sr composition $x = 0.066$, 0.171, and 0.276, respectively), which is expected from the interpolation between the relevant temperature coefficients of the binary PbSe and SrSe compounds.[7] Considering the fact that the band gaps in many ternary alloys can be approximated in the form of a quadratic function, we get

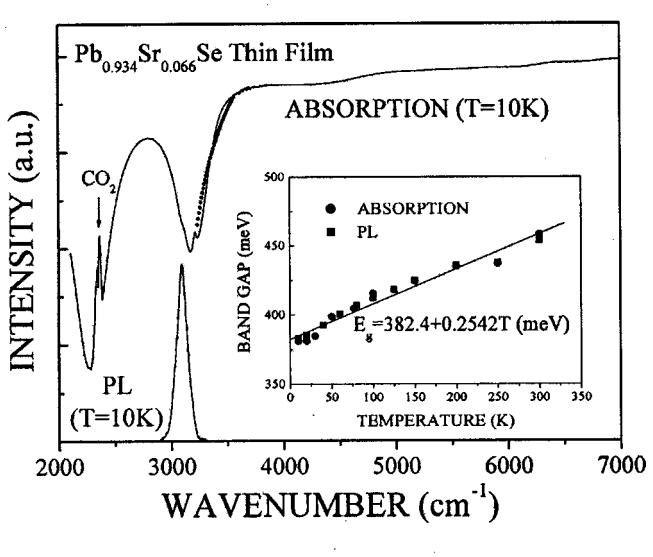

FIG. 1. Experimental photoluminescence (laser excitation intensity of 1.0 W/cm^2) and absorption spectra of a MBE grown $Pb_{0.934}Sr_{0.066}Se$ thin film at 10 K. The solid circles are the theoretical calculation of the absorption edge for effective masses from a six-band **k·p** model. Shown in the inset is the temperature-dependent band gaps of $Pb_{0.934}Sr_{0.066}Se$ thin film from photoluminescence and absorption measurements, together with a linear fit by the solid line.

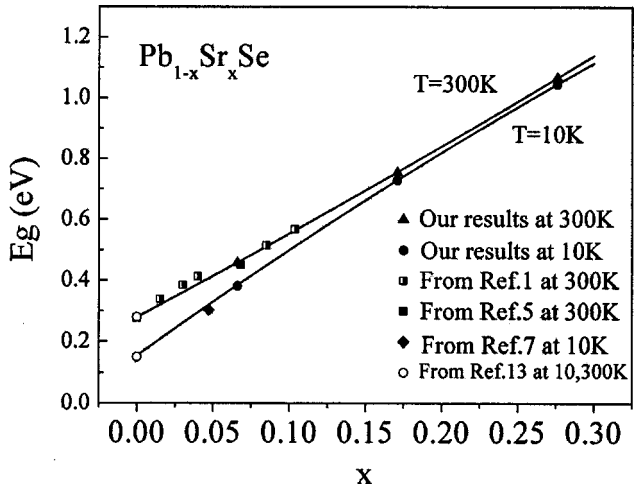

FIG. 2. Band gaps vs composition under the temperature of 10 and 300 K. The solid curves, given by Eq. (1), are the least square fitted results from our experiments. Previously reported band gap values from Refs. 1, 5, 7 and 13 are also included.

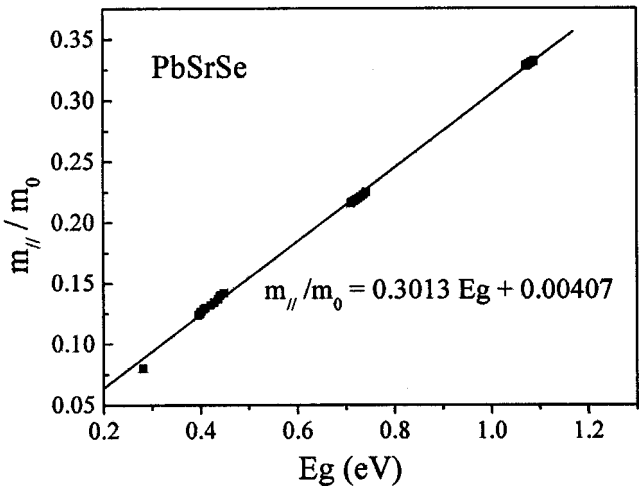

FIG. 3. Effective mass parallel to the [111] direction vs energy gaps E_g for PbSrSe thin films. Data obtained by varying E_g via composition and temperature are also included. The solid line, given by Eq. (3), is the linear fit to the results.

the empirical equation of Sr composition- and temperature-dependent band gaps $E_g(x,T)$ for $Pb_{1-x}Sr_xSe$ thin films based on our experimental results

$$E_g(x,T)=0.150+3.608x-1.314x^2+(0.430-3.093x+6.495x^2)\times 10^{-3}T \quad (\text{eV})$$
$$(\text{for } 0\leqslant x\leqslant 0.276,\ 0<T\leqslant 350\,\text{K}) \tag{1}$$

Figure 2 shows the band gaps as a function of Sr composition (x) at 10 and 300 K along with our experimental results and the results reported by other authors in the literature (Refs. 1, 5, 7 and 13). Curves by Eq. (1) in Fig. 2 match very well with both our experimental results and the reported data (including PbSe[13]) by different groups with different growth conditions, clearly demonstrating that band gaps of Eq. (1) are applicable to PbSrSe (and PbSe) thin films.

IV. EFFECTIVE MASSES IN PbSrSe

In IV–VI semiconductor materials, the valence band and conduction band are (nearly) symmetrical with similar dispersion in **k** space, and there is no heavy hole band in the system. These are the main differences between IV–VI and III–V materials. Holes in IV–VI materials such as PbSe have effective masses just as small as electrons, as evidence by similar carrier mobilities in *n*-type and *p*-type materials.[14] The mass anisotropy in **k** space (the ratio between longitudinal and transverse directions, $m_\parallel/m_\perp=1.8$, for PbSe and 3.0 for SrSe[7]) must be taken into account. As a special property of the **k·p** band models both the effective masses and the matrix element for the interaction with radiation are given by the same momentum matrix element (or by two matrix elements in the case of anisotropic bands). Therefore, the absorption edge can be expressed either in terms of the effective masses or in terms of the matrix elements. A six-band **k·p** model[15] which has the form

$$\alpha(E)=\frac{8\pi e^2\sqrt{Eg}}{\epsilon_0 h^2 c\sqrt{\epsilon_\infty}}\sqrt{m_\parallel}\sqrt{E/Eg-1}\,f(E)$$
$$\text{with}\quad f(E)=\frac{Eg^2}{2E^2}\left[1+\frac{E^2}{Eg^2}+\left(\frac{E}{Eg}-1\right)\left(\frac{2}{3}+\frac{E-Eg}{5Eg}\right)+2\frac{m_\perp}{m_\parallel}\left(\frac{E+Eg}{E}-\frac{2}{5}-\frac{E-Eg}{7Eg}\right)\right] \tag{2}$$

has been employed to calculate the absorption edge in PbSrSe thin films, shown as solid circles in Fig. 1. The mass anisotropy ratio for ternary PbSrSe was estimated from the binary ones by using a linear interpolation scheme. The resultant band gap is in good agreement with the above estimation from absorption and PL spectra with an error within 3%. From this model, we can also extract the effective masses for $Pb_{1-x}Sr_xSe$ thin films. Figure 3 displays the results for the effective masses parallel to the [111] direction, where data obtained by varying band gaps via composition as well as temperature have also been included. A linear least square fit to the results yields the empirical equation for the longitudinal $m_\parallel$

$$m_\parallel/m_0=0.3013\times E_g+0.00407 \quad (\text{for } 0.2\leqslant E_g\leqslant 1.2\,\text{eV}) \tag{3}$$

with m_0 as the free electron mass and E_g in the unit of eV. This expression is in good agreement with the results in Ref. 7 for small Sr composition, and for PbSe[13] as well. The result has also been used in the following calculation for $PbSe/Pb_{0.934}Sr_{0.066}Se$ MQW mid-infrared laser structures.

V. REFRACTIVE INDICES

The refractive index (n) data of PbSrSe thin films can be obtained from FTIR absorption measurements using the relation $n=(2\Delta\nu d)^{-1}$, with $\Delta\nu$ the spacing between Fabry-Pérot interference fringes and d the thickness of the MBE-grown PbSrSe thin films. The normal theoretical method for refractive index is based on the calculation of the imaginary

part of the dielectric constant $\epsilon_2(E)$, and on using the Kramers–Kronig relations to obtain the real part $\epsilon_1(E)$, using the relation $n(E)^2=\{[\epsilon_1(E)^2+\epsilon_2(E)^2]^{1/2}+\epsilon_1(E)\}/2$. In order to compare the experimental data with the theoretical results, and to generalize the empirical equations for $\epsilon_1(E)$ and $\epsilon_2(E)$ in PbSrSe thin films, we have also performed spectroscopic ellipsometry (SE) measurements on PbSrSe thin films. The SE technique measures functions of the Fresnel reflection coefficients, which then must be related to film parameters, such as film thickness, surface roughness, dielectric functions, etc, by using parametrized models. The model fitting for the SE measurements on $Pb_{0.724}Sr_{0.276}Sr$ at room temperature reveals that the thin film has an energy gap of 1.0644 eV and thickness of 1.0921 μm. These results are in excellent agreement with the band gap from Eq. (1) and the designed growth film thickness, respectively. By using the thin film thickness and the other three fitting parameters from SE: the transition peak energy E_0 of 1.0211 eV, the broadening term C of 3.0 eV and the amplitude constant A of 81.36 eV, we found that the experimental refractive indices agree well with the theoretical results, which are based on a single Lorentz transition model for $\epsilon_2(E)$ and the Forouhi and Bloomer[16] (F&B)-type Kramers–Kronig integration for $\epsilon_1(E)$

$$\epsilon_2(E)=2nk=\frac{AE_0CE}{(E^2-E_0^2)^2+C^2E^2}$$

$$\text{and}\qquad \epsilon_1(E)=\epsilon_1(\infty)+\frac{2}{\pi}P\int_{Eg}^{\infty}\frac{\xi\epsilon_2(\xi)}{\xi^2-E^2}d\xi, \tag{4}$$

where k is the extinction coefficient, the P stands for the Cauchy principal part of the integral. The detailed results from the SE measurements will be published elsewhere. Figure 4 shows the theoretical results (solid curve) calculated with the above values of the four parameters E_g, E_0, C and A via Eq. (4) and $\epsilon_1(\infty)$ of 2.45, and experimental data with the thicknesses d (solid squares) at room temperature (300 K). The good agreement is evident not only at room temperature, but also throughout the measured temperatures (see Fig. 4). The only changes for the 10 and 100 K results shown in Fig. 4 are the band gap E_g [via Eq. (1)] for the theoretical calculation, and the thin film thickness d for the experimental data. We have kept E_g-E_0 to be the constant of $1.0644-1.0211=0.0433$ eV in the calculation. From the resultant thin film thickness at different temperatures (also shown in Fig. 4), we can also obtain the thermal expansion coefficient for SrSe of $7.1\times10^{-6}\,K^{-1}$, if a linear interpolation scheme has been employed for the thermal expansion coefficient of PbSrSe from the binary SrSe and PbSe ($19.4\times10^{-6}\,K^{-1}$). This is the first known observation of the thermal expansion coefficient for SrSe.[2] Furthermore, $\epsilon_1(\infty)$ is found, from the comparison between experiment and theory, to obey

$$\epsilon_1(\infty)=2.45\quad(\text{for } E_g\geqslant 0.716\,\text{eV})$$

$$\text{and}\qquad 9.8-10.4\times E_g\quad(\text{for } E_g<0.716\,\text{eV}) \tag{5}$$

as shown in the inset of Fig. 5 with E_g in the unit of eV. The above derived thermal expansion coefficient for SrSe and the theoretical model of Eq. (4) are further verified in

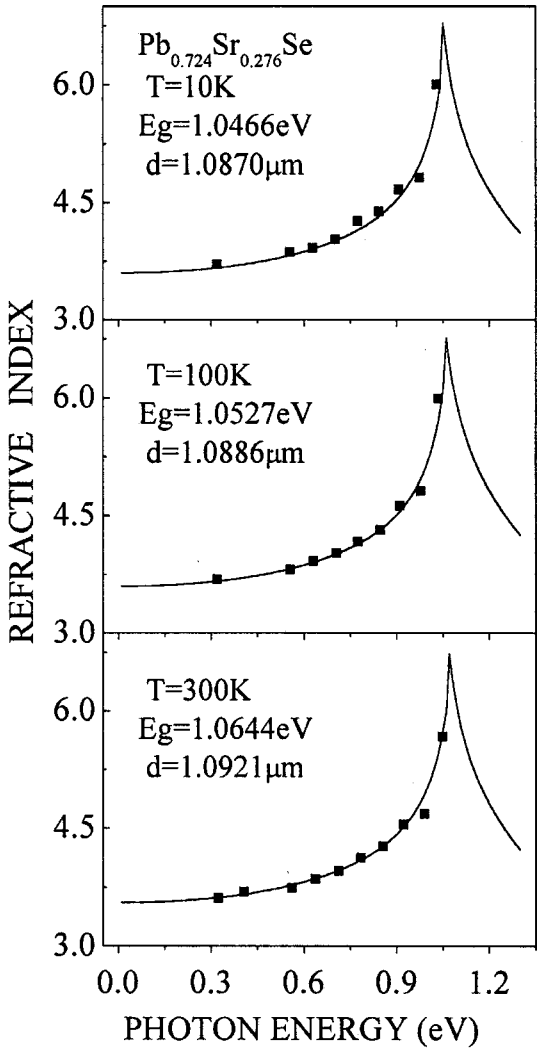

FIG. 4. Temperature-dependent refractive indices in $Pb_{0.724}Sr_{0.276}Se$ thin film as a function of photon energy. The theoretical results (solid curves) are calculated with the four parameters E_g, E_0, C and A via Eq. (4) and $\epsilon_1(\infty)$ of 2.45, together with the experimental data as solid squares.

temperature-dependent results of our other two PbSrSe thin films, with the only change of E_g [via Eq. (1)] and $\epsilon_1(\infty)$ [via Eq. (5)] in the theoretical calculation and thickness d in the experimental data. The obtained thermal expansion coefficient of SrSe is $(7.3\pm0.3)\times10^{-6}\,K^{-1}$. Further evidence for the theoretical model for PbSrSe thin films is shown in Fig. 5, where we have combined our experimental refractive indices (solid circles with $E_g=0.752$ eV) with the ones reported in Ref. 5 (filled squares with $E_g=0.577$ and 0.277 eV for PbSe) at room temperature. It should be noted that the theoretical model is also in good agreement with the results (filled triangles) in $PbSe/Pb_{0.934}Sr_{0.066}Se$ MQW laser systems[4] at photon energy above the band gap of PbSe due to the two-dimensional confinement. Thus, we have shown, through the consistency of all the observed experimental results, an easy way to calculate the refractive index in PbSrSe by combining Eqs. (1), (4) and (5) with the fitting parameters (A and C) given here.

The observed refractive index data in Figs. 4 and 5 show the expected increase in refractive index values as photon

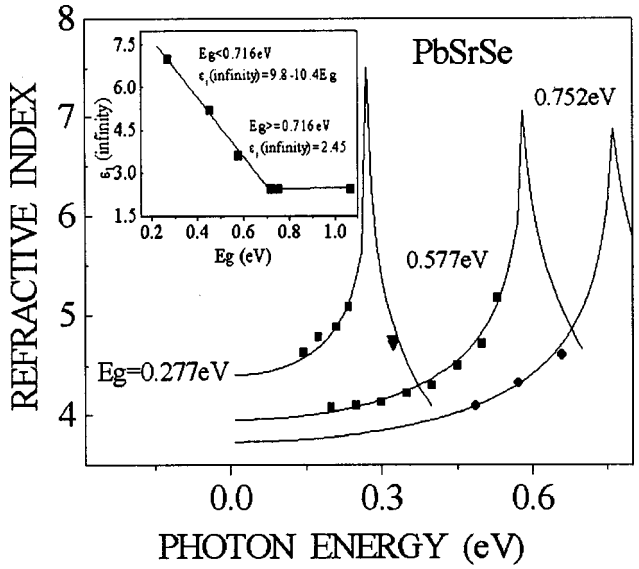

FIG. 5. Comparison of the theoretical model [Eqs. (4) and (5)] results for refractive index with the experimental refractive indices in PbSrSe thin films. Solid circles with $E_g = 0.752$ eV (our results), filled squares with $E_g = 0.577$ and 0.277 eV for PbSe in Ref. 5 at room temperature, and filled triangles for PbSe/$Pb_{0.934}Sr_{0.066}Se$ MQW laser systems[4] at photon energy above the band gap of PbSe due to the two-dimensional confinement. Shown in the inset is the band gap dependence of $\epsilon_1(\infty)$.

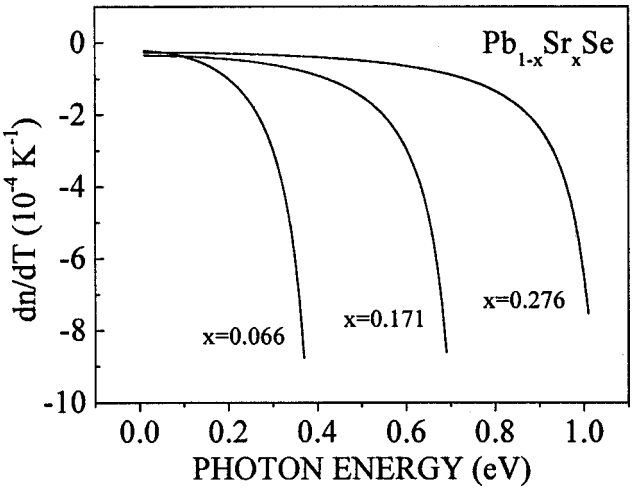

FIG. 6. The calculated temperature rate of the refractive index dn/dT as a function of photon energy below the band gap of the PbSrSe thin films.

energy increases to approach the band gap energy, and then decreases rapidly with further increase of the photon energy. The rapid change in refractive index near the band gap provides a large refractive index step between the active and cladding regions, suitable for laser design. It is also found, as expected, that smaller band gap PbSrSe thin films have larger refractive indices. The importance of the refractive index on the operation of an injection laser is its role in the confinement of the emitted radiation to the intermediate vicinity of the active region.[6] If the refractive index in the active region of an injection laser is smaller than that of the cladding layer on both sides, the effect is like that of an anti-waveguide configuration which does not confine radiation to the neighborhood of the active region. This effect causes an optical loss in the waveguide, leading to an increase of the threshold current. Another important factor for the refractive index study is the rate of refractive index change with temperature, dn/dT, from the temperature stability point of view of the optoelectronic devices. Figure 6 shows the calculated rate dn/dT [also via Eqs. (1), (4) and (5)] as a function of photon energy below the band gap of the PbSrSe thin films. The absolute value of the rate dn/dT is small ($<1.0 \times 10^{-4}\,K^{-1}$) at smaller photon energies and increases rapidly (in absolute value of dn/dT) as the photon energies approach the band gap. The temperature rate of refractive index near band gap is close to the value of $8.2\times10^{-4}\,K^{-1}$ in PbSe.[4] From the above discussion, it is clear that the refractive indices must be taken into account carefully in designing the PbSe/PbSrSe MQW laser structures, and our model provides the possibility of designing the laser structures with large index step and weak temperature rate dn/dT at emitted wavelength.

VI. APPLICATIONS

Now, we employ (and verify) the above analytical expressions for temperature-dependent band gaps and the composition (or band gap)-dependent effective masses in a PbSe/PbSrSe MQW mid-infrared laser system[4] with Sr composition of 0.066 to study the band offsets and the subband behavior, by taking into account the strain, carrier confinements and the multivalley band structure. The strain of the MQW structures is determined as the relative difference in lattice constants between the PbSe well ($a_{PbSe} = 6.127$ Å) and $Pb_{1-x}Sr_xSe$ ($a_{PbSrSe} = 6.137$ Å for $x = 0.066$) barrier layers. The latter is approximated as $a_{PbSrSe} = a_{PbSe}(1 + 0.025x)$ (Å).[1] In MQW cases, the PbSe wells will be expected to suffer a tensile strain of 1.65×10^{-3}, while the $Pb_{1-x}Sr_xSe$ barriers can be regarded as unstrained.[17] For the (111) growth direction, the strain-induced changes in the PbSe band structure for (111) transverse valley can be calculated to be 5.9 meV from the measured elastic constants and from calculated values of the deformation potentials of PbSe.[18] The value is in fair agreement with the experimental relationship between change in strain (0.21%) and change in band gap (6.2 meV) in PbSe.[11] The strain is approximated as being temperature independent due to the small fraction of Sr composition in the barriers, and the substrate-induced strain will not be considered in MQW since there are one 100-nm-thick BaF_2 and one very thick (~3 μm) PbSrSe buffer layers. The good agreement between theory and experiment shown below reveals that the lattice mismatch is entirely accommodated by strain in well layers without any relief by misfit dislocations present at the heterointerfaces. This also accounts for the strong room temperature luminescence in the MQW structures investigated.

In addition to the strain-induced renormalization of the energy bands, we should also take into account the electron and hole confinements for MQW structures, which are treated with standard procedures based on an application of the Kronig–Penny model with a parameter of conduction band offset ratio Q_c. Two sets of confinement energy levels, one associated with the (111) transverse valley and the other

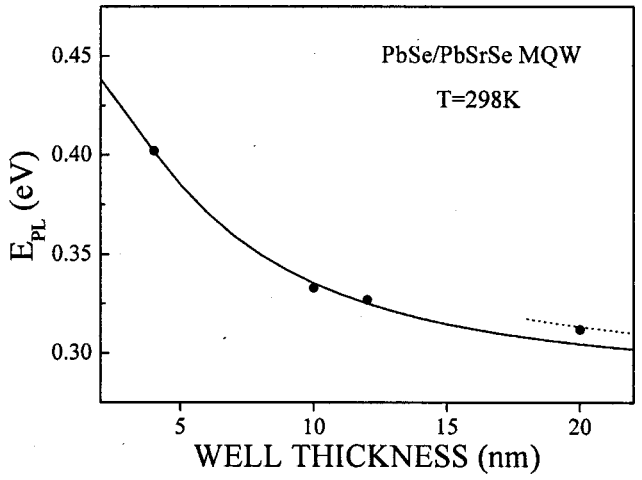

FIG. 7. Theoretical calculation of the luminescence peak energies (E_{PL}) for the (111) valley (solid curve) and ($\bar{1}11$) valleys (dotted curve) from $PbSe/Pb_{0.934}Sr_{0.066}Se$ MQW structures with $Q_c=0.82$ as a function of well thickness at 298 K. The solid circles are the experimental luminescence peak energies. The appearance of the ($\bar{1}11$) valleys for the 200 Å well structure is due to the fact that the lowest hole subband lies above the quasi-Fermi level there.

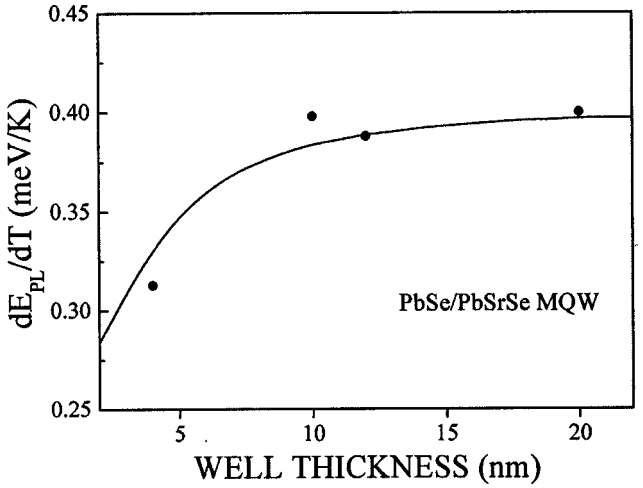

FIG. 8. Temperature coefficient of the luminescence peak energies (dE_{PL}/dT) from $PbSe/Pb_{0.934}Sr_{0.066}Se$ MQW structures as a function of well thickness. Solid curve: theoretical calculation results with $Q_c=0.82$, solid circles: experimental results.

with the three ($\bar{1}11$) oblique valleys, are obtained. These two set energy levels are close to each other for a given quantum number due to the small ellipsoidal mass anisotropy of PbSe and PbSrSe. The strong luminescence, observed even above room temperature, is consistent with both electrons and holes being confined in the PbSe wells, and supports the type I band alignment for this heterostructure. In the calculation, we have employed the effective masses and band gaps for PbSe wells and PbSrSe barriers from Eqs. (1) and (3). The best fit was found to be with the conduction band offset ratio $Q_c=0.82\pm0.03$. Figure 7 displays the calculated luminescence energies at 298 K [solid curve for the (111) valley and dotted curve for ($\bar{1}11$) valleys with $Q_c=0.82$] as a function of well thickness for the $PbSe/Pb_{0.934}Sr_{0.066}Se$ MQW structures, together with the experimental results[4] of well thickness of 40, 100, 120, and 200 Å shown by the solid circles. The measured transition energies for 40, 100, and 120 Å well structures are in good agreement with the calculation, which confirms the type I configuration in PbSe/PbSrSe MQW structures (favorable for laser applications). For a 100 Å PbSe well, the calculated lowest electron and hole energy levels of carriers in the (111) valley lie at $E_{1e}^{(111)}=31.0$ meV and $E_{1h}^{(111)}=18.4$ meV above and below the respective band edges of bulk PbSe and at $E_{1e}^{(\bar{1}11)}=40.1$ meV and $E_{1h}^{(\bar{1}11)}=20.6$ meV for carriers in the ($\bar{1}11$) valleys. The combined energies of the lowest electron and hole levels lying at about 49.4 meV in the (111) valley above the band gap of bulk PbSe are in good agreement with the observed luminescence peak in MQW, after taking into account the strain effect.

However, the calculated peak energies in the (111) valley for 200 Å PbSe well sample are always lower than that of the experimental result, no matter what the Q_c is. In this case, the energy levels in the ($\bar{1}11$) valleys may also have contributed to the luminescence structure. The MBE samples were undoped but grown under excess Se flux atmosphere, resulting in being slightly p type with a carrier concentration of $\sim1\times10^{17}\,\mathrm{cm}^{-3}$.[1] The quasi-Fermi energy is estimated to be $E_F=\hbar^2(3\pi^2p)^{2/3}/2m_h=13.6$ meV (referenced to the valence band edge) with hole effective mass of $0.06m_0$. Therefore, the lowest hole subband [$E_{1h}^{(111)}=11.4$ meV] of the ($\bar{1}11$) valleys for the 200 Å well structure lies above the quasi-Fermi level, and transitions between ($\bar{1}11$) valleys also make a contribution to the luminescence signal (not the case for the other three samples). The energy difference (7.7 meV) of the subband energies between the ($\bar{1}11$) valleys and (111) valley accounts reasonably well for the energy difference (~6.3 meV) between the theoretical and experimental results shown in Fig. 7 (see the dotted curve).

The band structures obtained above can explain not only the observed luminescence peaks in PbSe/PbSrSe MQW structures, but also the observed temperature coefficient of the luminescence peaks (dE_{PL}/dT). The calculated luminescence peak energies (in meV) are found to be linear with the temperature, as already experimentally demonstrated.[4] Figure 8 shows the theoretical calculation results of dE_{PL}/dT as a function of well thickness, together with the experimental results[4] for the four MQW samples (solid circles). It is clear that the rapid decrease of the temperature coefficient dE_{PL}/dT at narrow well MQW structures is mainly due to the strong dependence of the subband levels on well width, as a result of small temperature coefficient of the band gaps (dE_g/dT) of the $Pb_{0.934}Sr_{0.066}Se$ barriers. The information for the band structures of the PbSe/PbSrSe MQW can be used to design the double heterostructure lasers. Figure 9 shows the calculated luminescence peak energies as a function of temperature and well thickness [for 20 nm well structure we have used the results for ($\bar{1}11$) valleys]. The laser wavelength can be tuned by both the well thickness and the operating temperature. For example, a laser with 12 nm well structure is expected to have a tuning range from 5.17 to 3.79 μm with temperature from 77 to 300 K, and have a tuning range from 3.77 to 5.49 μm at 77 K with well thickness from

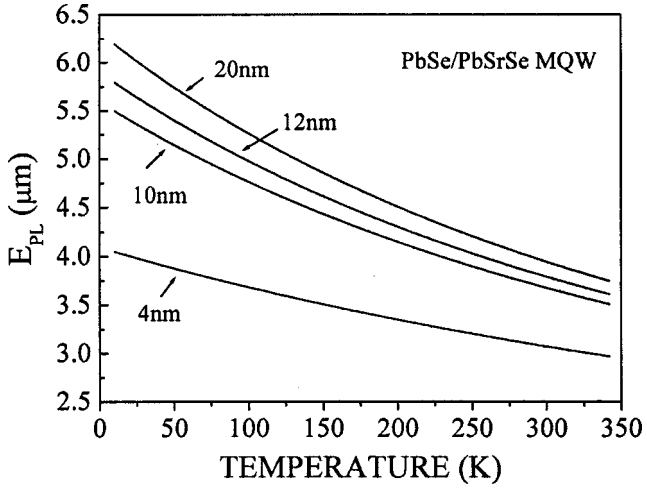

FIG. 9. Calculated luminescence peak energies (E_{PL} in μm, with $Q_c = 0.82$) from PbSe/$Pb_{0.934}Sr_{0.066}$Se MQW structures as a function of temperature under different well thickness. For 20 nm well structure we have used the results of $(\bar{1}11)$ valleys.

4 to 20 nm. Furthermore, one should also consider the refractive indices in the laser system by selecting the large index step and weak temperature rate dn/dT at the emitted wavelength, in order to obtain sufficient optical confinement. Since both the PL wavelength (Fig. 7 and temperature-dependent results in Fig. 8) and refractive indices (Fig. 5) from the laser structures,[4] together with the PbSrSe thin film results in the literature, have been shown to be in good agreement with our theoretical models, the present empirical equations [Eqs. (1), (3), (4), and (5)] provide an easy way to design optoelectronic devices based on PbSe/PbSrSe.

Finally, we discuss the origin of the luminescence structures in PbSe/PbSrSe MQW structures. The PL intensity was found[5] to increase with the temperature up to 170–210 K, and then decrease monotonically as the temperature increases, very similar to the case of PbSrSe thin films mentioned in Sec. III. Therefore, we can attribute the luminescence origin in PbSe/PbSrSe MQW structures to that of the PbSrSe thin films: localized excitonic transition below 170–210 K and band-to-band transitions at high temperature. The two-dimensional characteristics in PbSe/PbSrSe MQW structures are evident by delocalized temperature of 170–210 K and room temperature FWHM~40 meV, in comparison with 100 K and ~67.4 meV in PbSrSe thin films.

VII. CONCLUSIONS

In summary, PbSrSe thin films have attracted great interest because of their potential application in mid-infrared optoelectronic devices, especially in mid-infrared heterostructure lasers. A combined study of temperature-dependent photoluminescence and absorption measurements with theoretical models has been carried out on PbSrSe thin films for temperature-dependent band gaps, composition (or band gap)-dependent effective masses, and energy-dependent refractive indices. The derived empirical equations for band gaps, effective masses and refractive indices are in good agreement with the reported results in the literature and have been employed successfully by studying the band offsets and the subband behavior in PbSe/$Pb_{0.934}Sr_{0.066}$Se MQW mid-infrared laser systems. It is found that the thermal expansion coefficient of SrSe is $(7.3\pm0.3)\times10^{-6}\,K^{-1}$, and the PbSe/$Pb_{0.934}Sr_{0.066}$Se MQW structures are with type I band alignment and the conduction band offset ratio $Q_c = 0.82 \pm 0.03$. The good agreement with the reported experimental results in the literature clearly demonstrates that the results obtained here are applicable to other PbSrSe thin films and PbSe/PbSrSe heterostructure systems for their optoelectronic applications.

ACKNOWLEDGMENTS

This work is supported in part by the Natural Science Foundation of China under Contract No. 60006005, Shanghai QMX Project No. 00QA14012, and TRAPOYT project of Minister of Education (MOE), P. R. China. The authors would like to acknowledge L. G. Zhu and C. Y. Jin for their technical help.

[1] A. Lambrecht, N. Herres, B. Spanger, K. Kuhn, H. Böttner, M. Tacke, and J. Evers, J. Cryst. Growth **108**, 301 (1991).
[2] G. Xu, X. M. Fang, P. J. McCann, and Z. Shi, J. Cryst. Growth **209**, 763 (2000).
[3] P. Müller, H. Zogg, A. Fach, J. John, C. Paglino, A. N. Tiwari, M. Krejci, and G. Kostorz, Phys. Rev. Lett. **78**, 3007 (1997).
[4] P. J. McCann, K. Namjou, and X. M. Fang, Appl. Phys. Lett. **75**, 3608 (1999).
[5] X. M. Fang, K. Mamjou, I. N. Chao, P. J. McCann, N. Dai, and G. Tor, J. Vac. Sci. Technol. B **18**, 1720 (2000).
[6] H. C. Casey, Jr., and M. B. Panish, *Heterostructure Lasers* (Academic, New York, 1978), parts A and B.
[7] J. W. Tomm, K.-P. Möllmann, F. Peuker, K. H. Herrmann, H. Böttner, and M. Tacke, Semicond. Sci. Technol. **9**, 1033 (1994).
[8] W. Z. Shen, X. G. Wang, Z. G. Qian, L. F. Jiang, S. C. Shen, H. Z. Wu, and P. J. McCann, (unpublished).
[9] F. Fuchs and P. Koidl, Semicond. Sci. Technol. **6**, C71 (1991).
[10] P. J. McCann, L. Li, J. E. Furneaux, and R. Wright, Appl. Phys. Lett. **66**, 1355 (1995).
[11] H. K. Sacher, I. N. Chao, P. J. McCann, and X. M. Fang, J. Appl. Phys. **85**, 7398 (1999).
[12] J. H. Chu, S. Q. Xu, and D. Y. Tang, Appl. Phys. Lett. **43**, 1064 (1983).
[13] J. I. Pankove, *Optical Process in Semiconductors* (Dover, New York, 1975).
[14] P. J. McCann, S. Aanegola, and J. E. Furneaux, Appl. Phys. Lett. **65**, 2185 (1994).
[15] T. R. Globus, B. L. Gelmont, K. I. Gelman, V. A. Kondrashov, and A. V. Matveyenko, Sov. Phys. JETP **53**, 5 (1981).
[16] A. R. Forouhi and I. Bloomer, Phys. Rev. B **34**, 7018 (1986); **38**, 1865 (1988).
[17] W. Z. Shen, S. C. Shen, W. G. Tang, Y. Zhao, and A. Z. Li, Appl. Phys. Lett. **67**, 3432 (1995).
[18] S. Rabii, Phys. Rev. **167**, 801 (1968).